Structural Chemistry (2024) 35:1021–1029
https://doi.org/10.1007/s11224-023-02244-7

RESEARCH

Structural evolution and electronic properties of medium-sized $CrSi_n^{-/0}$ (n = 19–25) clusters

Kai Wang[1] · Chaoyong Wang[1] · Wei Li[1] · Le Liu[1] · Yarui Wang[1] · Jiaye Chen[1] · Jun Zhao[1] · Junji Guo[1]

Received: 15 September 2023 / Accepted: 12 October 2023 / Published online: 31 October 2023

Abstract

Herein, the structural evolution, electronic and magnetic properties of $CrSi_n^{-/0}$ for n = 19–25 have been investigated at density functional theory (DFT) level. The global minimum structures of these clusters have been fully searched through a self-developed genetic algorithm code combined with DFT calculations. Both of anionic and neutral $CrSi_n$ for n = 19–25 share the same configurations. All these clusters prefer to adopt endohedral structures ($Cr@Si_{14}$ for sizes n = 19–21, and $Cr@Si_{13}$ for larger ones) as the structural motif with the remaining Si atoms attached on the surface. Among all these clusters, $CrSi_{22}$ and $CrSi_{23}$ are the most prominent through the analysis of HOMO − LUMO gaps, average binding energies, and the second order of energy differences. All of these medium-sized cluster anions possess the same total magnetic moment of 1 μ_B, but with very different contributions from that of small sizes ($n \leq 18$), except for size 22.

Keywords Chromium-doped silicon clusters · Structural evolution · Density functional theory · Genetic algorithm

Introduction

Silicon clusters have potential applications in micro-nano devices as building blocks to continue the miniaturization trend of Moore's Law. However, the pure silicon clusters are always chemically reactive, limiting their applications [1, 2]. Fortunately, the introduction of transition metals into silicon clusters can significantly improve their stabilities [3–5], and may also introduce novel electronic and magnetic properties [6, 7], possibly allowing them to be used as building block for cluster-assembled materials. For example, the caged clusters of Si_{16} encapsulating a group-IV metal atom form superatoms with large HOMO–LUMO gaps [8–10]. The wheel-like $V_3Si_{12}^-$ cluster exhibits a ferromagnetic state with a total magnetic moments of 4μ_B [7]. Therefore, more and more experimental and theoretical efforts have been devoted to this type silicon clusters in recent thirty years [8–50]. In the early stages, people mainly studied the stability of these clusters through mass spectrometry technology. For example, Beck studied the stability of $TMSi_n$ (TM = Cr, Mo, W, Cu) clusters by mass spectrometry experiments, revealing several stable clusters including $TMSi_{15,16}$ (TM = Cr, $Mo^{0/+}$, W) [11, 12]. Neukermans et al. also studies a series of similar systems including $TMSi_n$ (TM = Cr, Mn, Cu, Zn) clusters through the similar mass spectrometry experiments [13]. Subsequently, more advanced technology such as photoelectron spectroscopy (PES) was used to investigate the electronic properties of a series of dopants (Sc, Ti, V, Y, Zr, Nb, Lu, Tb, Ho, Hf, Ta, Mo, and W) doped Si_n^- clusters with sizes $n \leq 20$ [14–18]. The demand for understanding the structure information of these type clusters urges the research on their structures. The structures of $MSi_{8\text{-}16}$ (M = Sc–Zn, Zr, Hf, Ta; $n \leq 18$) [19–28], $M_2Si_{1\text{-}8}$ (M = Cr, Mn, Fe, Co, Ni) [29, 30], $Mo_2Si_{9\text{-}16}$ [31], $M_2Si_{11\text{-}18}$ (M_2 = Mo_2, Nb_2, Ta_2, W_2, NbMo, TaW) [32], $Ag/AuSi_{10,12,14}$ [51], and $AuSi_{1\text{-}12}^{0/+}$ [52] clusters were predicted based on DFT calculations, and their structural evolutions is clarified accordingly. Considering the experimental photoelectron spectrum as the fingerprint of a cluster or molecule [53–55], the comparison of experimental and theoretical spectra have been used as criteria to identify the ground-state structures of $TMSi_n^-$ (TM = $Sc_{1\text{-}2}$ [33, 34], $V_{1\text{-}2}$ [35], $Cr_{1\text{-}2}$ [36, 37], Co [38], $Nb_{1\text{-}2}$ [39, 40], Ag [41], La [42], Ta [43], $Au_{1\text{-}2}$ [44, 45], $n \leq 14$; TM = $Ti_{1\text{-}2}$ [10], $V_{1\text{-}3}$ [46–48], $Cr_{1\text{-}2}$ [47, 49]; $14 \leq n \leq 20$) clusters in recent years. Both experimental

✉ Kai Wang
kkwangkai@huuc.edu.cn

[1] Henan Engineering Research Centre of Building-Photovoltaics, School of Mathematics and Physics, Henan University of Urban Construction, Pingdingshan 467036, China

and theoretical results show that TM atoms prefer to be surrounded by Si atoms, and forming endohedral structures with the growing number of Si atoms, except for TM = Cu, Ag and Au for small sizes with TM atoms absorbed on the surface of the bare Si_n clusters [41, 44, 50].

Among all 3d transition metals, chromium ($3d^5 4s^1$) is the only one has 6 unpaired electrons in the valence shell, making it an interesting dopant for the modulation of magnetic properties. Therefore, Cr-Si clusters have received widespread attention [36, 37, 47, 49, 56, 57] due to their potential applications in spintronic materials [58] and contact materials [59]. Recent studies have shown that small-sized $CrSi_n$ exhibits strange structures and magnetic properties [36, 37]. For example, $Cr_3Si_{12}^-$ possess a wheel-like structure [37]. Both of $Cr_2Si_{13}^-$ and $Cr_3Si_{12}^-$ exhibit large magnetic moments of $3\mu_B$ and $7\mu_B$, respectively [37]. Our recent research on $CrSi_{14-18}$ cluster anions shows that Cr atoms do not always contribute positive magnetic moments [47]. It is worth exploring the structural information and magnetic behaviors of Cr atoms in larger-sized clusters. Based on this, we conducted a systematically theoretical investigation on the structural evolution, electronic and magnetic properties of anionic and neutral $CrSi_n$ clusters for $n = 19–25$.

Computational method

The critical step in theoretical study of a cluster is to obtain its reliable structure. Therefore, low-lying structures of $CrSi_n^{-/0}$ ($n = 19–25$) clusters were globally searched through a self-developed genetic algorithm code incorporated with the ORCA 5.0.4 software [60, 61] for DFT calculations. For each size, more than 3000 configurations were generated by the genetic algorithm code to fully search on the potential energy surface. The validity and efficiency of our global optimization algorithm code have been well demonstrated by several of our recent works about $TMSi_{14-20}^-$ (TM = V_{1-3}, Cr_{1-2}) [46–49], $TMGe_{8-17}^-$ (TM = Ti-Ta) [62], and $In_{3-16}X_{0,1}^-$ (X = Si, Ge) [63], $Cr_2Ge_{15-20}^-$ [64], $CsSi_{5-16}^-$ [65], and Ge_{4-30}^- [66] clusters. Considering that the scheme of BP86 functional with Karlsruhe-type basis sets has proven to be suitable for the description of structural evolution and electronic properties of $Cr_{1-2}Si_{14-20}^-$ and $Cr_2Ge_{15-20}^-$ clusters in our previous works [47, 49, 64], therefore, this scheme was also adopted for the calculations of $CrSi_n^{-/0}$ ($n = 19–25$) clusters. Briefly, the def2-SVP basis set [67, 68] and the BP86 functional [69, 70] were adopted for DFT calculations during the global search. Then the higher-quality def2-TZVP basis set [67, 68] was employed to further optimize the top 10–20 candidate isomers to get more accurate geometric structures, and the diffuse def2-TZVP basis set (def2-TZVPD) [71] was adopted to obtain more accurate energies. All the structures have positive vibrational frequencies from vibration analyses. Zero-point-energy corrections were considered for the energy calculations. Various spin multiplicities (SM) were considered in order to obtain the lowest-energy spin state. The vertical detachment energy (VDE) was obtained from the energy differences between the anionic and neutral clusters at the relaxed structure of the anionic state. The adiabatic detachment energy (ADE) were calculated as the energy differences between the anionic cluster and the relaxed neutral clusters using the anionic structure as initial configuration.

The stabilities of anionic and neutral $CrSi_n$ cluster are evaluated by the average binding energies (E_b) defined as Eqs. (1) and (2) [72, 73]:

$$E_b(CrSi_n^-) = [(n-1)E(Si) + E(Si^-) + E(Cr) - E(CrSi_n^-)]/(n+1) \quad (1)$$

$$E_b(CrSi_n) = [nE(Si) + E(Cr) - E(CrSi_n)]/(n+1) \quad (2)$$

where $E(CrSi_n^-)$ and $E(CrSi_n)$is the energies of the anionic and neutral $CrSi_n$ clusters, respectively; $E(Si)$, $E(Si^-)$ and $E(Cr)$ are the total energies of the neutral Si, anionic Si and neutral Cr atoms, respectively. The second order of energy difference ($\Delta_2 E$) of a $CrSi_n^{-/0}$ was calculated using the formula (3):

$$\Delta_2 E(CrSi_n^{-/0}) = E(CrSi_n^{-/0}) + E(CrSi_n^{-/0}) - 2E(CrSi_n^{-/0}) \quad (3)$$

All the graphs of the structures of clusters involved in this work were rendered by using the molecular graphics program VMD 1.9.3 [74]. The average bond length, Wiberg bond order, and electron spin density were calculated by using the post processing program of Multiwfn 3.8 (dev) [75].

Computational results

Structures of $CrSi_n^{-/0}$ ($n = 19 – 25$) clusters

The optimized structures of first three lowest-lying isomers of anionic and neutral $CrSi_{19-25}$ at the BP86/def2-TZVP level are displayed in Fig. 1. The calculations show that there are four typical endohedral structures (see Fig. 2) as the motifs in these low-lying isomers of $CrSi_{19-25}^{-/0}$ clusters. These motifs are also adopted for $TMSi_{14}$ (TM = Mn, Fe, Co) [76], $TiSi_{17-20}^-$ [10], and VSi_{16-20}^- [46], and $CrSi_{16-18}^-$ [49] clusters.

For anionic $CrSi_n^-$ clusters, the lowest-energy isomers (*n*As) prefer to adopt endohedral structures (motif I (Cr@Si_{14}) for sizes $n = 19–21$, and motif IV (Cr@Si_{13}) for larger ones) as the structural motif with the extra Si atoms attached on the surface. The lowest-energy structures of $CrSi_{19}^-$ and $CrSi_{20}^-$ also are adopted for VSi_{19}^- and VSi_{20}^- clusters, respectively [46]. Motif I is adopted for isomers 21B, 21C,

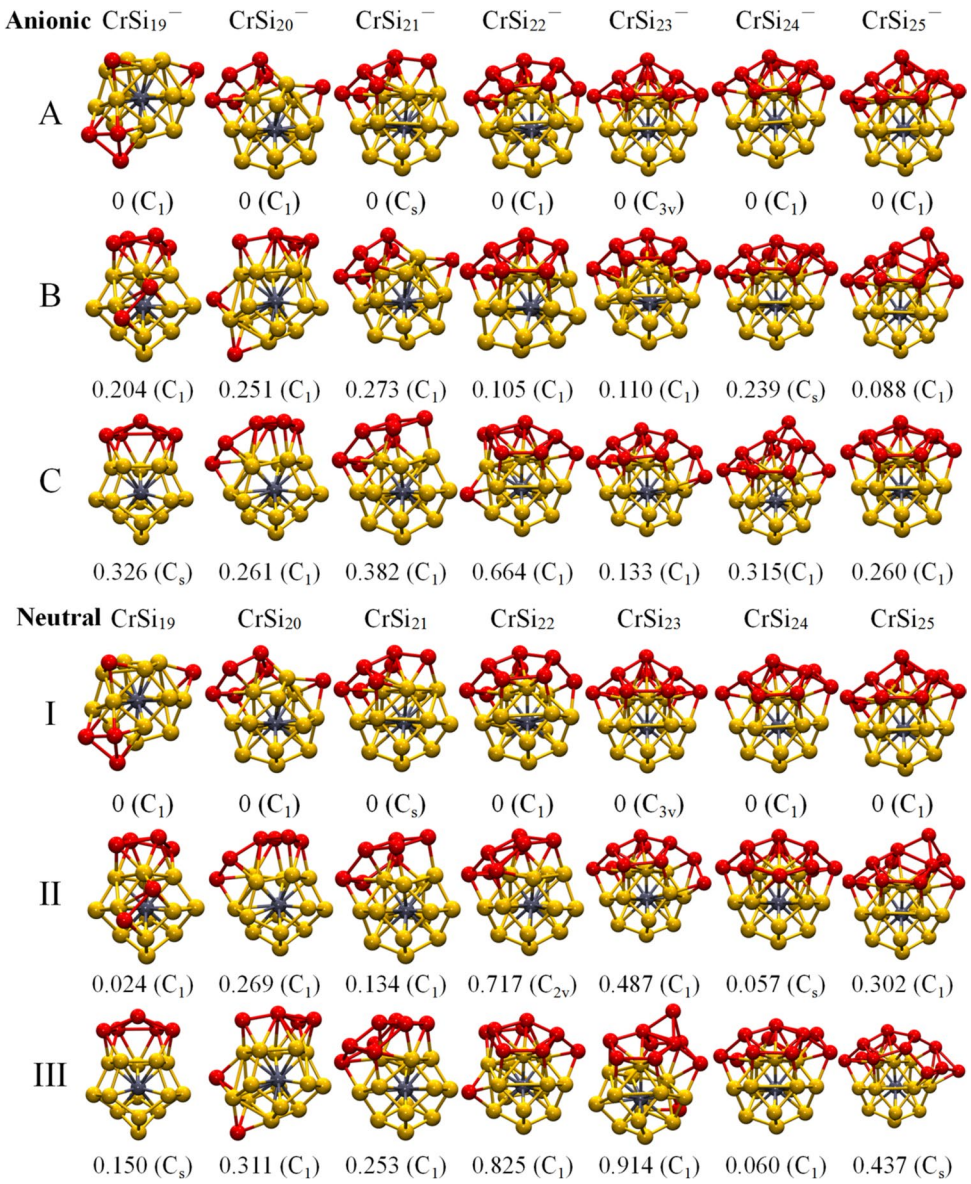

Fig. 1 Geometric structures of low-energy isomers for $CrSi_{19\text{-}25}^{-/0}$ clusters. For each size, the total energy difference (eV) with respect to the lowest-lying isomer is provided below the structure, and the symmetry is given inside the parentheses. Gray balls represent chromium atoms. The silicon atoms formed a cage and adsorbed on the surface are highlighted as yellow and red, respectively

and 22B as the core structural motif with excess Si atoms attached to the surface, showing the strong dominance in size range of $n = 19$–21. Starting from size 22, the dominance of motif I begins to weaken, instead, motif IV begins to show high competitiveness, which is adopted for all the first three isomers for sizes $n = 23$–25. The motif of isomer 19B is also

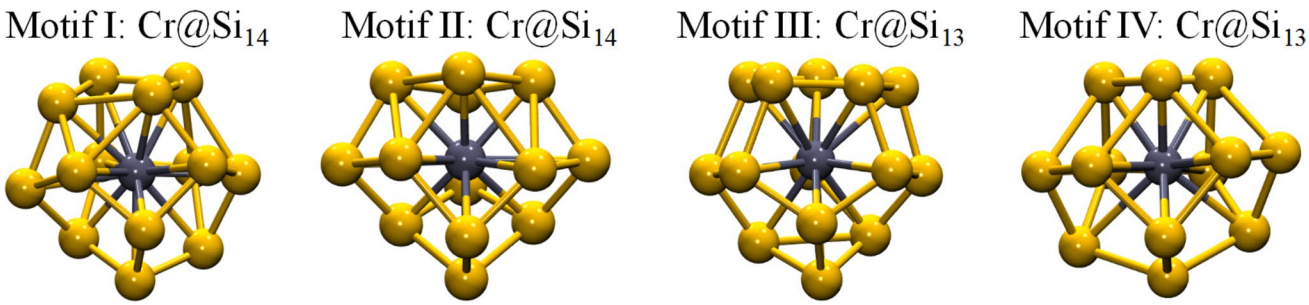

Fig. 2 Four typical structural motifs present in isomers of $CrSi_n$ clusters with $n = 19$–25 taken from isomers 19A, 22A, 19B, and 20C, respectively. Motifs II and III can be generated from motifs I and IV by removing one of the top Si atoms, respectively

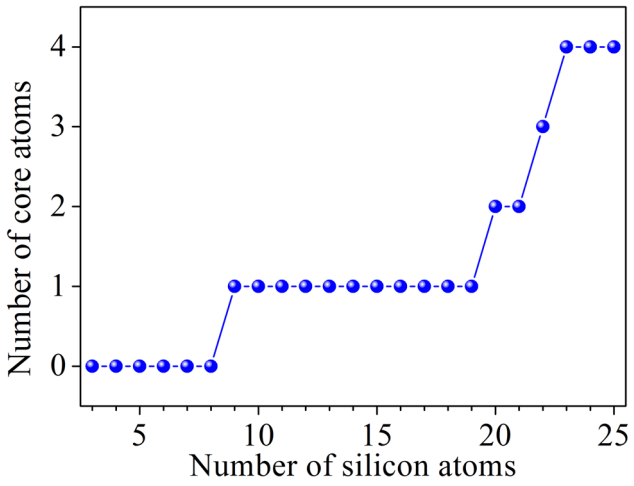

Fig. 3 A plot showing the core evolution in the lowest-energy isomers of $CrSi_n$ (n = 3–25) clusters. Gray and yellow balls represent chromium and silicon atoms, respectively. The results for sizes n = 3–18 are from previous works [36, 49, 78]

an endohedral $Cr@Si_{13}$ structure (motif II), which is also adopted for $TMSi_{14}$ (TM = Mn, Fe, Co) clusters [76]. The motif III always represents a building block ($Cr@Si_{14}$) for the ground-state $TMSi_n$ (TM = Ti^-, $V^-$and Cr^- for n = 17, 18 [10, 44, 49]) clusters, but is only adopted by isomers 19C, 20B and 20C among all these isomers for n = 19–21, indicating its weak competitiveness in large size clusters.

For neutral $CrSi_n$ (n = 19–25) clusters, their structures are very similar to that of anionic states. All the lowest-energy isomers of neutral $CrSi_n$ (n = 19–25) share the same configurations as that of anionic state. The calculated results (see Table S3 of Supplementary materials) show that all the root mean square deviations (RMSD) of anionic and neutral states are small with less than 0.13 Å, except for sizes 20 and 22 with values of 0.221 Å and 0.215 Å, respectively. This result indicates that the reduction of one electron in an anionic system has little effect on its geometric structure. Isomers 19II and 19III of neutral $CrSi_{19}$ adopt the same configurations as 19B and 19C of anionic state, respectively. Isomers 20II, 20III, 21II, 22III, 23II, 24III, and 25II, adopt the same configurations as 20C, 20B, 21C, 22C, 23C, 24B, and 25B, respectively. Isomers 22II and 23III adopt the motif I, while 24II and 25III are based on the motif IV with excess Si atoms absorbed on the surface.

For sizes n = 21–25 for $CrSi_n^{-/0}$ clusters, each successive cluster size is composed of its predecessor with an extra Si atom adsorbed onto the surface, giving evidence of a stepwise growth. Moreover, the core also increases with the cluster size (see Fig. 3). Single Cr atom as core first observed in $CrSi_9$ still exists in $CrSi_{19}$, but for larger sizes, the clusters prefer to grow by core expansion. Both of the global minimum $CrSi_{20}$ and $CrSi_{21}$ possess a two-atom core, while $CrSi_{22}$ has a three-atom core. The four-atom core of $CrSi_{23}$ is a tetrahedral bipyramid and is persistent in the global minima of sizes n = 23–25. Significantly, the structure of $CrSi_{23}$ is very similar to the smallest core–shell silicon cluster Si_{27}^- [77], indicating that Cr atom accelerate the formation of cage-like structure for pure silicon cluster. From another point of view, the influence of Cr atom on the structure of pure silicon cluster starts to weaken.

Photoelectron spectra of $CrSi_n^-$ (n = 19 – 25) clusters

Figure 4 shows the simulated PES for the lowest-energy isomers of $CrSi_n^-$ (n = 19–25) cluster anions. For $CrSi_{19}^-$, the spectrum possesses six distinguishable peaks at 3.29, 3.65, 3.79, 4.11, 4.44 and 4.69 eV. In the PES of $CrSi_{20}^-$, there are two small peaks at 3.31 and 3.57 eV, followed by four prominent peaks located at 3.87, 4.26, 4.46, and 4.79 eV. For $CrSi_{21}^-$, the first peak locates at 3.29 eV, followed by three high-intensity peaks centered at 3.89, 4.13, and 4.59 eV. Similar spectrum is also observed in $CrSi_{22}^-$, the PES also possesses a clear small peak at 3.48 eV, followed by three prominent peaks located at 3.85, 4.21, and 4.49 eV. In the case of $CrSi_{23}^-$, there is a large separation between the highest occupied state and (2.92 eV) the next lower-lying state (3.87 eV), indicating a large gap between the highest occupied state (HOMO) and the lowest unoccupied state (LUMO) of the corresponding neutral cluster. This result corresponds to the large HOMO–LUMO gap of 1.50 eV for neutral $CrSi_{23}$. Similar to $CrSi_{23}^-$, the simulated spectrum of $CrSi_{24}^-$ also has a small peak at 3.10 eV and three prominent peaks situated at 3.73, 4.13, and 4.45 eV. For $CrSi_{25}^-$, four discrete peaks are located at 3.12, 3.41, 3.77, and 4.30 eV, respectively. In short, for the simulated PES of $CrSi_n^-$ (n = 19–25) clusters, the spectral characteristics and peak positions are obviously different, indicating their significant differences in electronic properties. The

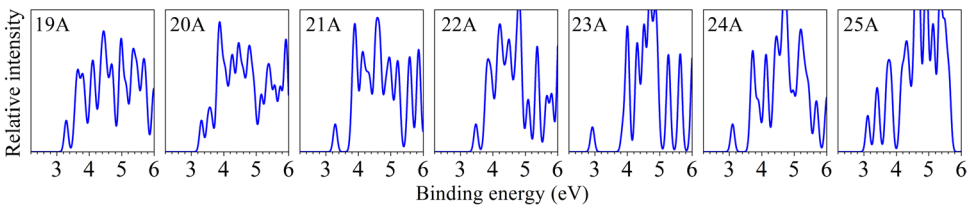

Fig. 4 Theoretical photoelectron spectra of the lowest-lying isomers of $CrSi_n^-$ (n = 19–25). Gaussian broadening with a width of 0.06 eV is used

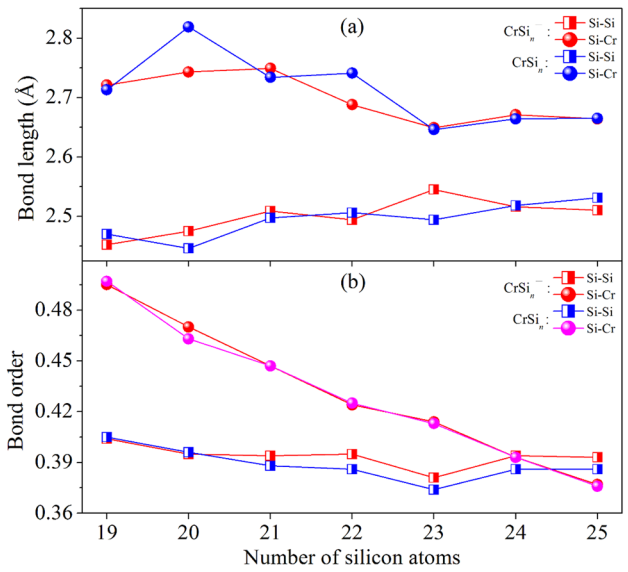

Fig. 5 Average bond lengths (**a**) and Wiberg bond orders (**b**) of Si–Si and Si-Cr of the lowest-energy structures of $CrSi_n^{-/0}$ ($n = 19$–25) clusters

simulated PESs are expected to provide some guidance for future PES measurements.

Bonding and electronic properties of $CrSi_n^{-/0}$ ($n = 19$ – 25) clusters

To further explore the bonding and electronic properties of the $CrSi_n^{-/0}$ ($n = 19$–25) clusters, the average bond lengths, Wiberg bond orders, vertical detachment energies (VDEs), adiabatic detachment energies (ADE), HOMO–LUMO gaps, average binding energies (E_b), and the second order of energy difference (Δ_2E) for the lowest-energy structures were calculated and presented in Figs. 5 and 6 as well as summarized in Table 1.

From Fig. 5, the average bond length and bond order of Si–Si and Si-Cr bonds in anionic state are close to those in the neutral state. From Fig. 5(a), the average Si-Cr bond lengths (2.649 Å–2.819 Å) have significantly larger values than that of Si–Si bonds in the range of 2.446 Å–2.545 Å. The Wiberg bond orders (Fig. 5b) of Si-Cr bonds show a gradual decrease trend for $CrSi_n^{-/0}$ ($n = 19$–25) clusters in

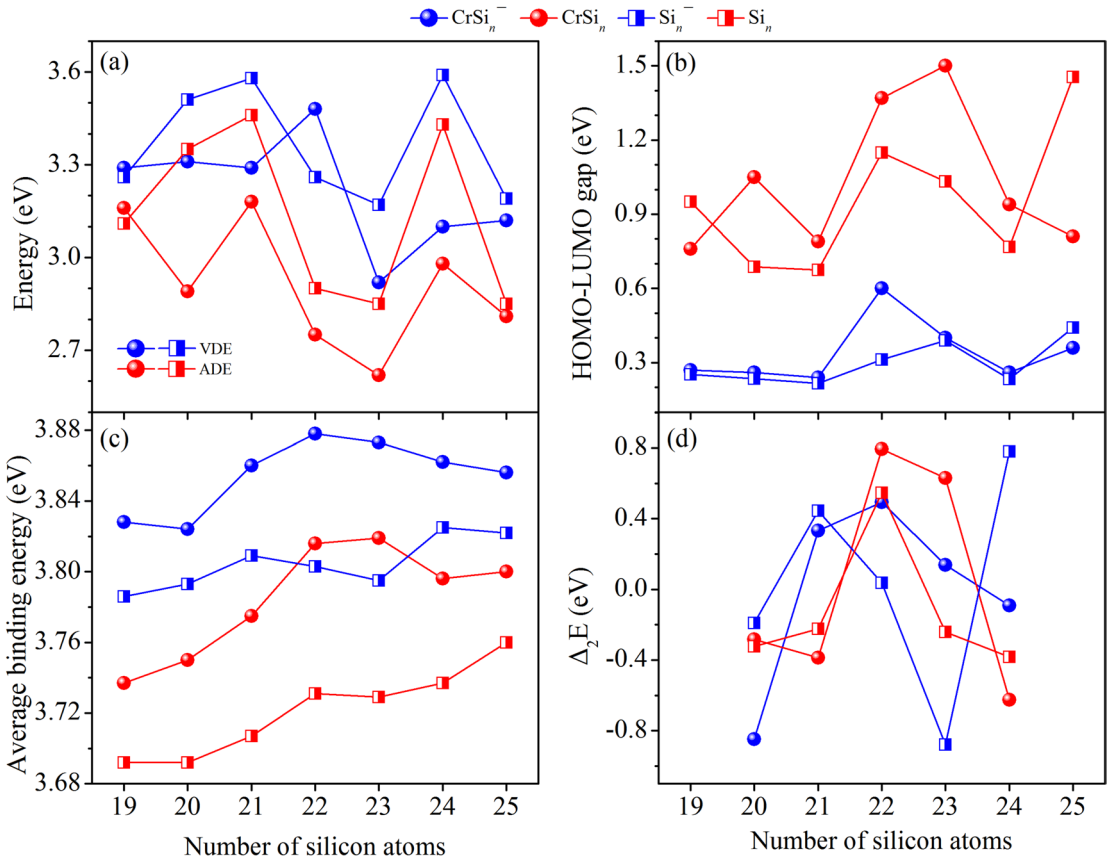

Fig. 6 Size-dependent vertical detachment energies (VDE), adiabatic detachment energies (ADE), HOMO − LUMO gaps, binding energies (E_b), and second order of energy difference (Δ_2E) of the lowest-lying structures of $CrSi_{19\text{-}25}^{-/0}$ clusters with the results of $Si_{19\text{-}25}^{-/0}$ for comparison. The ground-state structures of $Si_{19\text{-}25}$ clusters are from previous works [77, 79]

Table 1 Spin multiplicities (SM), average bond lengths (BL, in Å), bond orders (BO), vertical detachment energies (VDE, in eV), adiabatic detachment energies (ADE, in eV), HOMO − LUMO gaps (E_{HL}, in eV), average binding energies (E_b, in eV), and the second order of energy difference (Δ_2E, in eV) of the lowest-energy structures of $CrSi_n^{-/0}$ (n = 19–25) clusters

Size	SM	BL		BO		VDE	ADE	E_{HL}	E_b	Δ_2E
		Si–Si	Si-Cr	Si–Si	Si-Cr					
$CrSi_{19}^-$	2	2.452	2.721	0.404	0.495	3.29		0.27	3.828	
$CrSi_{20}^-$	2	2.475	2.743	0.395	0.470	3.31		0.26	3.824	-0.848
$CrSi_{21}^-$	2	2.509	2.749	0.394	0.447	3.29		0.24	3.860	0.333
$CrSi_{22}^-$	2	2.494	2.688	0.395	0.424	3.48		0.60	3.878	0.494
$CrSi_{23}^-$	2	2.545	2.649	0.381	0.414	2.92		0.40	3.873	0.138
$CrSi_{24}^-$	2	2.516	2.671	0.394	0.393	3.10		0.26	3.862	-0.092
$CrSi_{25}^-$	2	2.510	2.664	0.393	0.377	3.12		0.36	3.856	
$CrSi_{19}$	1	2.470	2.713	0.405	0.497		3.16	0.76	3.737	
$CrSi_{20}$	1	2.446	2.819	0.396	0.463		2.89	1.05	3.750	-0.283
$CrSi_{21}$	1	2.497	2.734	0.388	0.447		3.18	0.79	3.775	-0.387
$CrSi_{22}$	1	2.506	2.741	0.386	0.425		2.75	1.37	3.816	0.794
$CrSi_{23}$	1	2.494	2.646	0.374	0.413		2.62	1.50	3.819	0.631
$CrSi_{24}$	1	2.518	2.664	0.386	0.393		2.98	0.94	3.796	-0.625
$CrSi_{25}$	1	2.531	2.665	0.386	0.376		2.81	0.81	3.800	

range of 0.495–0.376, while that of Si–Si bond fluctuate in a small size range of 0.374–0.405.

It shows that the VDEs (Fig. 6a) of $CrSi_n^-$ are very close for n = 19 to 21, rise to 3.48 eV at n = 22, and then abruptly drop to 2.92 eV at n = 23, gradually rising up again from n = 24 to 25. The trend of ADEs of $CrSi_n$ is roughly consistent with that of VDE, except for sizes 20 and 22, which corresponds to the large root mean square deviations (RMSD, see Fig. S3) values of anionic and neutral structures. The trend of VDE of Si_n^- is roughly consistent with that of ADE for Si_n. All the ADE and VDE values for neutral and anionic Si_n are bigger than that of $CrSi_n$ clusters, except for sizes 19 and 22, respectively. This result indicates that Cr atoms can usually reduce the detachment energy of silicon cluster.

The trend of the HOMO–LUMO gaps for $CrSi_n^-$ (in Fig. 6b) is similar to that of the VDE, except for size 23. The HOMO–LUMO gap of neutral $CrSi_n$ and Si_n clusters are significantly larger than that of anionic states. This is because there are unpaired electrons in the anionic states. It is worth noting that the neutral $CrSi_{22}$ and $CrSi_{23}$ have large HOMO–LUMO gaps of 1.37 eV and 1.50 eV, respectively. All the HOMO–LUMO gap values for neutral and anionic $CrSi_n$ are bigger than that of Si_n clusters, except for sizes 19 and 25. It is worth noting that the influence of Cr atoms on the HOMO–LUMO gap value of Si_n^- is generally very small, but for the neutral state.

From Fig. 6c, the average binding energies (E_b) exhibit similar trends in both anionic and neutral $CrSi_n$ and Si_n clusters. E_b of $CrSi_n^-$ for sizes 19 and 20 are significantly lower than that of larger sizes, increase gradually until coming to the maximum at n = 22, and then decrease monotonously. For neutral $CrSi_n$ clusters, the largest value of E_b occurs in size 23. Compared with pure Si_n clusters, $CrSi_n$ clusters have a larger average binding energy, which is consistent with our expected results that doping transition metals can improve the stability of pure silicon clusters.

Interestingly, the trends of the Δ_2E (Fig. 6d) of $CrSi_n^-$ and Si_n^- clusters are consistent with that of average binding energy curves. $CrSi_{22}^-$ and $CrSi_{22}$ also possess the largest Δ_2E values, indicating the largest relative stabilities. For anionic and neutral Si clusters, their local maximum values occur at sizes 21 and 22, respectively. Significantly, the $CrSi_{22}$ and $CrSi_{23}$ clusters have the considerable HOMO–LUMO gap, E_b, and Δ_2E values in the neutral and anionic states, respectively. The results indicate that these two clusters have high stabilities among these clusters.

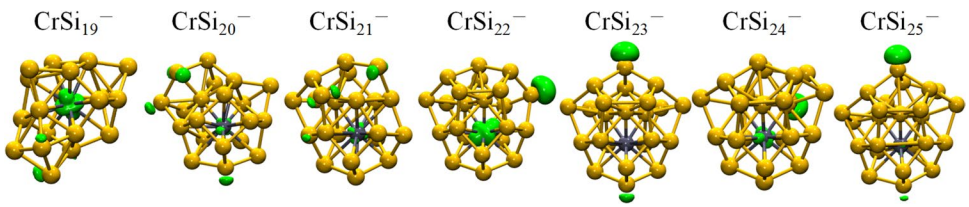

Fig. 7 Isosurface maps of the electron spin density of the lowest-energy $CrSi_{19\text{-}25}^-$ clusters. The isosurface is set to ± 0.006 e/Å^3. Green and red isosurfaces indicate the positive and negative electron spin density, respectively

Table 2 The total magnetic moments (μ_T) of the $CrSi_{19-25}^-$ clusters were obtained by Hirshfeld population analysis, along with the local magnetic moment on the Cr atom (μ_{Cr}) and the Si atom with the maximum value ($\mu_{Si\text{-}Max}$). All magnetic moments are in μ_B

Cluster	μ_T	μ_{Cr}	$\mu_{Si\text{-}Max}$
$CrSi_{19}^-$	1	0.31	0.13
$CrSi_{20}^-$	1	0.07	0.18
$CrSi_{21}^-$	1	0.08	0.16
$CrSi_{22}^-$	1	0.55	0.40
$CrSi_{23}^-$	1	-0.04	0.36
$CrSi_{24}^-$	1	0.12	0.26
$CrSi_{25}^-$	1	0.01	0.34

Magnetic properties of $CrSi_n^-$ ($n = 19 – 25$) clusters

Our results (see Tables S1 and S2 in Supplementary materials) show that all these of anionic and neutral $CrSi_{19-25}$ clusters are in their lowest spin states, therefore, we just explore the magnetic properties of the $CrSi_{19-25}^-$ cluster anions by the calculations of spin electron density and Hirshfeld population. The results are displayed in Fig. 7 and listed in Table 2, respectively. From Fig. 7, one can see that the green zones (the excess alpha electrons) appear around the Cr atom and some Si atoms with low coordination number, while the red regions (the excess beta electrons) are hardly distributed. Different from the results that Cr atoms in small-sized $CrSi_n^-$ ($n \leq 18$) clusters [49] contribute most of the total magnetic moments of 1 μ_B, their contributions in larger clusters are not significant, even less than that of some Si atoms, except for size 22 with $\mu_{Cr} = 0.55$ μ_B. This result indicates that the source of magnetic moment changes obviously for larger sized clusters studied here, which may be related to the saturation of Cr atoms.

Conclusions

The structural evolution, electronic and magnetic properties of $CrSi_{19-25}^{-/0}$ clusters have been computationally investigated. Global research for of the minimum structures of these clusters have been performed on a self-developed genetic algorithm code combined with DFT calculations. All the anionic $CrSi_n^-$ clusters share the same configurations as that of their neutral states for $n = 19–25$. All these $CrSi_{19-25}^{-/0}$ clusters prefer to adopt endohedral structures ($Cr@Si_{14}$ for sizes $n = 19–21$, and $Cr@Si_{13}$ for $n = 22–25$) as the structural motif with the remaining Si atoms attached on the surface. The simulated photoelectron spectra show that these clusters have obvious size dependence. From the average binding energy results, the doping Cr atoms can significantly improve the stabilities of the pure silicon clusters. Among all these clusters, both of $CrSi_{22}$ and $CrSi_{23}$ possess large HOMO – LUMO gaps, average binding energies, and the second order of energy differences, indicating their high stabilities. All of the clusters possess total magnetic moment of 1 μ_B, but with very different contributions from that of small sizes ($n \leq 18$), except for size 22.

Supplementary Information The online version contains supplementary material available at https://doi.org/10.1007/s11224-023-02244-7.

Author contributions K.W. wrote the manuscript. K. W., C. W., W. L., L. L., Y. W., J. C., J. Z. and J. G. analyzed the data and discussed the results. K. W. conceived the project, designed and supervised the whole research. K.W. revised and edited the manuscript. All authors contributed to the manuscript preparation.

Funding This work is financially supported by the Scientific research start-up fund for high-end talents of Henan University of Urban Construction (Grant No. K-Q2023048) and Key Research Project Plan for Higher Education Institutions in Henan Province (Grant No. 23A140026).

Availability of data and materials See the supplementary material for relative energies (Tables S1 and S2) of the $CrSi_{19-25}^{-/0}$ clusters anion for three different spin multiplicities (SM). The root mean square deviations of the lowest-energy isomers of anionic and neutral $CrSi_{18-25}$ clusters were summarized in Table S3. The theoretical photoelectron spectra of the top three lowest-lying isomers of $CrSi_n^-$ ($n = 19–25$) were shown in Fig. S1. Mulliken population analysis results of magnetic moments for $CrSi_n^-$ ($n = 19–25$) were summarized in Table S4. The natural electron configuration of Cr atoms for $CrSi_{19-25}^-$ clusters were shown in Table S5. The comparison of photoelectron spectra for $CrSi_{19-25}^-$ and Si_{19-25}^- clusters were shown in Fig. S3. The calculated data of electronic properties for Si_{19-25}^- and Si_{19-25} were summarized in Table S6. Relative energies of the top three lowest-energy structures of $CrSi_n^{-/0}$ ($n = 19–25$) for the three different functionals were listed in Table S7.

Declarations

Ethical approval This declaration is not applicable.

Competing interests The authors declare no competing interests.

References

1. Röthlisberger U, Andreoni W, Parrinello M (1994) Structure of nanoscale silicon clusters. Phys Rev Lett 72:665–668
2. Ho KM, Shvartsburg AA, Pan B, Lu ZY, Wang CZ, Wacker JG, Fye JL, Jarrold MF (1998) Structures of medium-sized silicon clusters. Nature 392:582
3. Zhao J, Du Q, Zhou S, Kumar V (2020) Endohedrally doped cage clusters. Chem Rev 120:9021–9163
4. Jena P, Sun Q (2018) Super atomic clusters: Design rules and potential for building blocks of materials. Chem Rev 118:5755–5870
5. Farooq U, Naz S, Xu H-G, Yang B, Xu X-L, Zheng W-J (2020) Recent progress in theoretical and experimental studies of metal-doped silicon clusters: Trend among elements of periodic table. Coord Chem Rev 403:213095
6. Huang X, Xu H-G, Lu S, Su Y, King RB, Zhao J, Zheng W (2014) Discovery of a silicon-based ferrimagnetic wheel structure in $V_xSi_{12}^-$ ($x = 1–3$) clusters: photoelectron spectroscopy and density functional theory investigation. Nanoscale 6:14617–14621
7. Yang B, Xu H, Xu X, Zheng W (2018) Photoelectron spectroscopy and theoretical study of $Cr_nSi_{15-n}^-$ (n = 1–3): Effects of doping Cr atoms on the structural and magnetic properties. J Phys Chem A 122:9886–9893

8. Reis CL, Pacheco JM (2010) Bulk materials made of silicon cage clusters doped with Ti, Zr, or Hf. J Phys Condens Mat 22:035501
9. Wu X, Zhou S, Huang X, Chen M, Bruce King R, Zhao J (2018) Revisit of Large-Gap Si_{16} Clusters Encapsulating Group-IV Metal Atoms (Ti, Zr, Hf). J Comput Chem 39:2268–2272
10. Wu X, Du Q, Zhou S, Huang X, Chen M, Miao L, Yin G, Wang J, Wang K, von Issendorff B, Ma L, Zhao J (2020) Structures, stabilities and electronic properties of $Ti_mSi_n^-$ (m = 1–2, n = 14–20) clusters: a combined ab initio and experimental study. Eur Phys J Plus 135:734
11. Beck SM (1987) Studies of silicon cluster–metal atom compound formation in a supersonic molecular beam. J Chem Phys 87:4233–4234
12. Beck SM (1989) Mixed metal–silicon clusters formed by chemical reaction in a supersonic molecular beam: Implications for reactions at the metal/silicon interface. J Chem Phys 90:6306–6312
13. Neukermans S, Wang X, Veldeman N, Janssens E, Silverans RE, Lievens P (2006) Mass spectrometric stability study of binary MS_n clusters (S=Si, Ge, Sn, Pb, and M=Cr, Mn, Cu, Zn). Int J Mass Spectrom 252:145–150
14. Ohara M, Koyasu K, Nakajima A, Kaya K (2003) Geometric and electronic structures of metal (M)-doped silicon clusters (M=Ti, Hf, Mo and W). Chem Phys Lett 371:490–497
15. Koyasu K, Akutsu M, Mitsui M, Nakajima A (2005) Selective Formation of MSi_{16} (M = Sc, Ti, and V). J Am Chem Soc 127:4998–4999
16. Koyasu K, Atobe J, Akutsu M, Mitsui M, Nakajima A (2007) Electronic and geometric stabilities of clusters with transition metal encapsulated by silicon. J Phys Chem A 111:42–49
17. Furuse S, Koyasu K, Atobe J, Nakajima A (2008) Experimental and theoretical characterization of MSi_{16}^-, MGe_{16}^-, $MS_{n1}{}^6-$, and $MP_{b1}{}^6-$ (M=Ti, Zr, and Hf): The role of cage aromaticity. J Chem Phys 129:064311
18. Koyasu K, Atobe J, Furuse S, Nakajima A (2008) Anion photoelectron spectroscopy of transition metal- and lanthanide metal-silicon clusters: MSi_n^- (n=6–20). J Chem Phys 129:214301
19. Guo L-j, Zhao G-f, Gu Y-z, Liu X, Zeng Z (2008) Density-functional investigation of metal-silicon cage clusters MSi_n (M=Sc, Ti, V, Cr, Mn, Fe Co, Ni, Cu, Zn; n=8-16). Phys Rev B 77:195417
20. Kawamura H, Kumar V, Kawazoe Y (2005) Growth behavior of metal-doped silicon clusters Si_nM (M=Ti, Zr, Hf; n=8-16). Phys Rev B 71:075423
21. Torres MB, Fernández EM, Balbás LC (2007) Theoretical study of isoelectronic Si_nM clusters (M=Sc-, Ti, V+; n=14-18). Phys Rev B 75:205425
22. Kawamura H, Kumar V, Kawazoe Y (2004) Growth, magic behavior, and electronic and vibrational properties of Cr-doped Si clusters. Phys Rev B 70:245433
23. Li J-R, Wang G-H, Yao C-H, Mu Y-W, Wan J-G, Han M (2009) Structures and magnetic properties of Si_nMn (n=1–15) clusters. J Chem Phys 130:164514
24. Ma L, Wang J, Wang G (2013) Site-specific analysis of dipole polarizabilities of heterogeneous systems: Iron-doped Si_n (n = 1–14) clusters. J Chem Phys 138:094304
25. Ma L, Zhao J, Wang J, Wang B, Lu Q, Wang G (2006) Growth behavior and magnetic properties of Si_nFe (n=2-14) clusters. Phys Rev B 73:125439
26. Ma L, Zhao J, Wang J, Lu Q, Zhu L, Wang G (2005) Structure and electronic properties of cobalt atoms encapsulated in Si_n (n=1–13) clusters. Chem Phys Lett 411:279–284
27. Wang J, Ma Q-M, Xie Z, Liu Y, Li Y-C (2007) From Si_nNi to Ni@Si_n: An investigation of configurations and electronic structure. Phys Rev B 76:035406
28. Guo P, Ren Z-Y, Yang AP, Han J-G, Bian J, Wang G-H (2006) Relativistic computational investigation: The geometries and electronic properties of $TaSi_n^+$ (n = 1–13, 16) clusters. J Phys Chem A 110:7453–7460
29. Robles R, Khanna SN, Castleman AW (2008) Stability and magnetic properties of T_2Si_n (T=Cr, Mn, 1≤n≤8) clusters. Phys Rev B 77:235441
30. Robles R, Khanna SN (2009) Stable T_2Si_n (T=Fe Co, Ni,1≤n≤8) cluster motifs. J Chem Phys 130:164313
31. Han J-G, Zhao R-N, Duan Y (2007) Geometries, Stabilities, and Growth Patterns of the Bimetal Mo2-doped Si_n (n = 9–16) Clusters: A Density Functional Investigation. J Phys Chem A 111:2148–2155
32. Pham HT, Phan Dang C-T, Duong LV, Tuyn PT, Nguyen MT (2022) Growth pattern of doubly metal doped silicon clusters M_2Si_n with $M_2 = Mo_2$, Nb_2, Ta_2, W_2, NbMo, TaW and n = 11–18. Formation of fused cages M_2Si_{18}. Chem Phys Lett 787:139229
33. Xu Hong-Guang WM-M, Zeng-Guang Z, Qiang S, Wei-Jun Z (2011) Structural and bonding properties of $ScSi_n$ (n=2~6) clusters: photoelectron spectroscopy and density functional calculations. Chin Phys B 20:43102–043102
34. Xu H-G, Zhang Z-G, Feng Y, Zheng W (2010) Photoelectron spectroscopy and density-functional study of $Sc_2Si_n^-$ (n=2–6) clusters. Chem Phys Lett 498:22–26
35. Xu H-G, Zhang Z-G, Feng Y, Yuan J, Zhao Y, Zheng W (2010) Vanadium-doped small silicon clusters: Photoelectron spectroscopy and density-functional calculations. Chem Phys Lett 487:204–208
36. Kong X, Xu H-G, Zheng W (2012) Structures and magnetic properties of $CrSi_n^-$ (n = 3–12) clusters: Photoelectron spectroscopy and density functional calculations. J Chem Phys 137:064307
37. Yang B, Xu X-L, Zheng W-J, Xu H-G (2022) Structural evolution and bonding properties of $Cr_2Si_n^-$ (n = 1–12) clusters: Mass-selected anion photoelectron spectroscopy and theoretical calculations. J Phys Chem A 126:1182–1193
38. Yang B, Xu X-L, Xu H-G, Farooq U, Zheng W-J (2019) Structural evolution and electronic properties of $CoSi_n^-$ (n = 3–12) clusters: mass-selected anion photoelectron spectroscopy and quantum chemistry calculations. Phys Chem Chem Phys 21:6207–6215
39. Lu S-J, Cao G-J, Xu X-L, Xu H-G, Zheng W-J (2016) The structural and electronic properties of $NbSi_n^{-/0}$ (n = 3–12) clusters: anion photoelectron spectroscopy and ab initio calculations. Nanoscale 8:19769–19778
40. Lu S-J, Xu H-G, Xu X-L, Zheng W-J (2017) Anion photoelectron spectroscopy and theoretical investigation on $Nb_2Si_n^{-/0}$ (n = 2–12) clusters. J Phys Chem C 121:11851–11861
41. Kong X-Y, Deng X-J, Xu H-G, Yang Z, Xu X-L, Zheng W-J (2013) Photoelectron spectroscopy and density functional calculations of $AgSi_n^-$ (n = 3–12) clusters. J Chem Phys 138:244312
42. Dai W-S, Yang B, Yan S-T, Xu H-G, Xu X-L, Zheng W-J (2021) Structural and electronic properties of $LaSi_n^{-/0}$ (n = 2–6) clusters: Anion photoelectron spectroscopy and density functional calculations. J Phys Chem A 125:10557–10567
43. Lu S-J, Xu H-G, Xu X-L, Zheng W-J (2020) Structural evolution and electronic properties of $TaSi_n^{-/0}$ (n = 2–15) clusters: Size-selected anion photoelectron spectroscopy and theoretical calculations. J Phys Chem A 124:9818–9831
44. Lu S-J, Xu X-L, Feng G, Xu H-G, Zheng W-J (2016) Structural and electronic properties of $AuSi_n^-$ (n = 4–12) clusters: Photoelectron spectroscopy and Ab initio calculations. J Phys Chem C 120:25628–25637
45. Lu S-J, Xu X-L, Xu H-G, Zheng W-J (2018) Structural evolution and bonding properties of $Au_2Si_n^{-/0}$ (n = 1–7) clusters: Anion photoelectron spectroscopy and theoretical calculations. J Chem Phys 148:244306
46. Wang K, Jia Z-Z, Fan Z, Zhao H-Y, Yin G-J, Moro R, von Issendorff B, Ma L (2022) Structures and electronic properties of

VSi_n^- (n = 14–20) clusters: a combined experimental and density functional theory study. Phys Chem Chem Phys 24:8839–8845
47. Wang K, Yin G-J, Jia Z-Z, Miao L, Moro R, von Issendorff B, Ma L (2022) Anion photoelectron spectroscopy and density functional theory study of $TM_2Si_n^-$ (TM = V, Cr; n = 14–20) clusters. Phys Chem Chem Phys 24:18321–18330
48. Wang K, Yin GJ, Jia ZZ, Miao L, Zhao HY, Moro R, von Issendorff B, Ma L (2023) Structural evolution, electronic and magnetic properties investigation of $V_3Si_n^-$ (n = 14–18) clusters based on photoelectron spectroscopy and density functional theory calculations. Chem Phys Lett 820:140423
49. Wang K, Zhao H-Y, Miao L, Jia Z-Z, Yin G-J, Zhu X-D, Moro R, von Issendorff B, Ma L (2022) Photoelectron spectroscopy and density functional investigation of the structural evolution, electronic, and magnetic properties of $CrSi_n^-$ (n = 14–18) clusters. J Phys Chem A 126:1329–1335
50. Xu H-G, Wu MM, Zhang Z-G, Yuan J, Sun Q, Zheng W (2012) Photoelectron spectroscopy and density functional calculations of $CuSi_n^-$ (n = 4–18) clusters. J Chem Phys 136:104308
51. Trivedi R, Bandyopadhyay D (2018) Evolution of electronic and vibrational properties of $M@X_n$ (M = Ag, Au, X = Ge, Si, n=10, 12, 14) clusters: a density functional modeling. J Mater Sci 53:8263–8273
52. Ranjan P, Chakraborty T (2020) A comparative study of structure, stabilities and electronic properties of neutral and cationic $[AuSi_n]^\lambda$ and $[Si_{n+1}]^\lambda$ (λ = 0, +1; n=1–12) nanoalloy clusters. Mater Today Commun 22:100832
53. Kostko O, Huber B, Moseler M, von Issendorff B (2007) Structure determination of medium-sized sodium clusters. Phys Rev Lett 98:043401
54. Huber B, Moseler M, Kostko O, von Issendorff B (2009) Structural evolution of the sodium cluster anions $Na_{20}^-Na5_{7-}$. Phys Rev B 80:235425
55. Ma L, von Issendorff B, Aguado A (2010) Photoelectron spectroscopy of cold aluminum cluster anions: Comparison with density functional theory results. J Chem Phys 132:104303
56. Han JG, Hagelberg F (2001) A density functional theory investigation of $CrSi_n$ (n = 1–6) clusters. Chem Phys 263:255–262
57. Tran VT (2020) Geometric and electronic structures of $CrSi_n^{-/0/+}$ (n = 1–3) clusters from DMRG-CASPT2 calculations. Chem Phys Lett 785:139166
58. Nie Z, Guo P, Zheng J, Zhao P, Wan Y, Jiang Z (2018) Electronic and magnetic properties of two dimensional cluster-assembled materials based on $TM@Si_{12}$ (TM = 3d transition metal) clusters. Comp Mater Sci 146:134–142
59. Chang MT, Chen CY, Chou LJ, Chen LJ (2009) Core−shell chromium silicide−silicon nanopillars: A contact material for future nanosystems. ACS Nano 3:3776
60. Neese F, Wennmohs F, Becker U, Riplinger C (2020) The ORCA quantum chemistry program package. J Chem Phys 152:224108
61. Neese F (2022) Software update: The ORCA program system—Version 5.0. Wires Comput Mol Sci 12:e1606
62. Wang K, Jia Z-Z, Wang R-Y, Zhu X-D, Moro R, Ma L (2022) $TMGe_{8\text{-}17}^-$ (TM = Ti, Zr, Hf, V, Nb, Ta) clusters: group determined properties. Eur Phys J Plus 137:949
63. Wang K, Miao L, Jia Z, Wang R, Yin G, Zhu X, Moro R, Ma L (2022) Structural evolution and electronic properties of pure and semiconductor atom doped in clusters: In_n^-, In_nSi^-, and In_nGe^- (n = 3–16). J Comput Chem 43:1978–1984
64. Wang K (2023) $Cr_2Ge_n^-$ (n = 15–20) clusters with two Cr atoms exhibited antiferromagnetic coupling. J Comput Chem 44:1667–1672
65. Wang K, Xu S, Li W, Chen S, Zhao Y (2023) Study the structures and electronic properties of $CsSi_n^-$ (n = 5–16) clusters by ab initio global search. Struct Chem. https://doi.org/10.1007/s11224-023-02203-2
66. Wang K, Wang C, Li W (2023) Structure determination of Ge_n^- (n= 4–30) clusters. Eur Phys J Plus 138:740
67. Weigend F, Ahlrichs R (2005) Balanced basis sets of split valence, triple zeta valence and quadruple zeta valence quality for H to Rn: Design and assessment of accuracy. Phys Chem Chem Phys 7:3297–3305
68. Weigend F (2006) Accurate Coulomb-fitting basis sets for H to Rn. Phys Chem Chem Phys 8:1057–1065
69. Perdew JP (1986) Density-functional approximation for the correlation energy of the inhomogeneous electron gas. Phys Rev B 33:8822–8824
70. Becke AD (1988) Density-functional exchange-energy approximation with correct asymptotic behavior. Phys Rev A 38:3098–3100
71. Rappoport D, Furche F (2010) Property-optimized Gaussian basis sets for molecular response calculations. J Chem Phys 133:134105
72. Trivedi R, Banerjee A, Bandyopadhyay D (2022) Insight into stabilities and magnetism of $EuGe_n$ (n = 1–20) nanoclusters: an assessment of electronic aromaticity. J Mater Sci 57:19338–19355
73. Trivedi R, Dhaka K, Bandyopadhyay D (2014) Study of electronic properties, stabilities and magnetic quenching of molybdenum-doped germanium clusters: a density functional investigation. RSC Adv 4:64825–64834
74. Humphrey W, Dalke A, Schulten K (1996) VMD: Visual molecular dynamics. J Mole Graph 14:33–38
75. Lu T, Chen F (2012) Multiwfn: A multifunctional wavefunction analyzer. J Comput Chem 33:580–592
76. He J, Wu K, Liu C, Sa R (2009) Stabilities of 3d transition-metal doped Si_{14} clusters. Chem Phys Lett 483:30–34
77. Bai J, Cui LF, Wang J, Yoo S, Li X, Jellinek J, Koehler C, Frauenheim T, Wang LS, Zeng XC (2006) Structural evolution of anionic silicon clusters Si_n ($20 \le N \le 45$). J Phys Chem A 110:908–912
78. Abreu MB, Reber AC, Khanna SN (2014) Does the 18-electron rule apply to $CrSi_{12}$? J Phys Chem Lett 5:3492–3496
79. Wu X, Liang XQ, Du QY, Zhao JJ, Chen MD, Lin M, Wang JS, Yin GJ, Ma L, King RB, Von Issendorff B (2018) Medium-sized Si_n^- (n = 14–20) clusters: a combined study of photoelectron spectroscopy and DFT calculations. J Phys Condens Matter 30:354002